Inorganic Chemistry

Article

pubs.acs.org/IC

An Anionic N-Donor Ligand Promotes Manganese-Catalyzed Water Oxidation

Karin J. Young, Michael K. Takase, and Gary W. Brudvig*

Department of Chemistry, Yale University, New Haven, Connecticut 06520, United States

Supporting Information

ABSTRACT: Four manganese complexes of pentadentate ligands have been studied for their ability to act as oxygen evolution catalysts in the presence of Oxone or hydrogen peroxide. The complexes $[Mn(PaPy_3)(NO_3)](ClO_4)$ (**1**) ($PaPy_3H$ = *N*,*N*-bis(2-pyridylmethyl)-amine-*N*-ethyl-2-pyridine-2-carboxamide) and $[Mn(PaPy_3)(\mu\text{-}O)(PaPy_3)Mn](ClO_4)_2$ (**2**) feature an anionic carboxamido ligand *trans* to the labile sixth coordination site, while [Mn(N4Py)OTf](OTf) (**3**) (N4Py = *N*,*N*-bis(2-pyridylmethyl)-*N*-bis(2-pyridyl)methylamine) and $[Mn(PY5)(OH_2)](ClO_4)_2$ (**4**) (PY5 = 2,6-bis(bis(2-pyridyl)methoxymethane)-pyridine) have neutral ligands of varying flexibility. **1** and **2** are shown to evolve oxygen in the presence of either Oxone or hydrogen peroxide, but **3** evolves oxygen only in the presence of hydrogen peroxide. **4** is inactive. The activity of **1** and **2** with Oxone suggests that the presence of an anionic N-donor ligand plays a role in stabilizing putative high-valent intermediates. Anionic N-donor ligands may be viewed as alternatives to μ-oxo ligands that are prone to protonation in low-valent Mn species formed during a catalytic cycle, resulting in loss of catalyst structure.

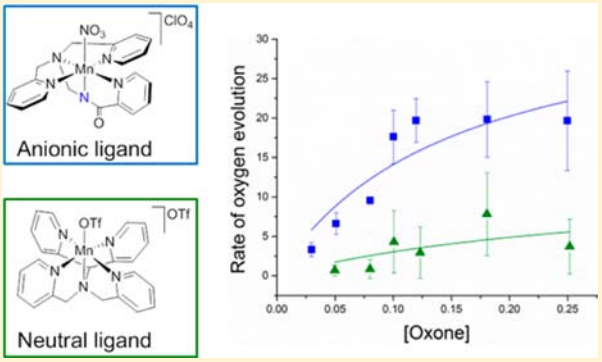

INTRODUCTION

The active site for water oxidation in photosystem II (PSII), the oxygen-evolving complex (OEC), is composed of a Mn_4CaO_x core that is conserved among higher plants and cyanobacteria.[1] During the course of enzyme turnover, the tightly coupled manganese centers of the OEC store four oxidizing equivalents generated sequentially by four light-driven charge separation events in PSII. After four oxidizing equivalents are accumulated, two oxygen atoms derived from water are coupled to form dioxygen. The critical O−O bond-forming step in PSII is believed to proceed by nucleophilic attack of water on an electrophilic Mn^{IV}—oxyl species.[1,2] Functional modeling of the water-oxidation chemistry of PSII is required as a component of artificial processes to convert sunlight into reducing equivalents for the formation of chemical fuels that may be used to harvest solar energy to meet growing global energy demand.[3,4]

While many structural models of the OEC have been prepared, only a few functional, molecular manganese water-oxidation catalysts are known.[5,6] Most of these catalysts are dinuclear, oxo-bridged complexes that require two-electron oxo donor oxidants for oxygen evolution, but a more recent example employs the oxidant $Ru(bpy)_3^{3+}$, where bpy = 2,2′-bipyridine.[7] Perhaps the most extensively studied example is $[Mn(tpy)(\mu\text{-}O)(OH_2)]_2(NO_3)_3$, where tpy = 2,2′;6′,2″-terpyridine, which is competent for oxygen evolution with Oxone ($KHSO_5$).[8,9] Consistent with available mechanistic and computational data, the O−O bond-forming step proceeds through nucleophilic attack of a solvent water on a high-valent Mn^{IV}—oxyl.[10,11] However, after dioxygen is released, the complex is reduced by four electrons to a Mn^{III}/Mn^{II} species. It is likely that the bridging oxo groups are susceptible to protonation in this low-valent state, causing the dimer to dissociate. Oxidation of the Mn^{III}/Mn^{II} species is needed to complete the catalytic cycle, but failure of the dimer to reassemble may be one decomposition pathway.

In order to improve the reactivity of manganese coordination compounds as water-oxidation catalysts, the ligand environment should be designed to promote formation of the electrophilic, high-valent Mn−oxo species required for O−O bond formation. In the manganese−terpyridine dimer described above, the bridging oxo groups are strong σ-donor ligands that stabilize Mn in higher-valent states. Other strong donor groups have also been employed to generate high-valent manganese species. Lomoth et al. report a Mn^{III}/Mn^{III} dimer supported by three phenolate ligands that stabilize the Mn^{IV}/Mn^{IV} state compared to a similar ligand without anionic donor groups.[12] Similarly, McKenzie and co-workers report a manganese dimer with a dangling carboxylate group that is active for oxygen evolution with *tert*-butyl hydrogen peroxide.[13,14] A similar ligand has been shown by Berggren et al. to form a manganese tetramer that oxidizes water in the presence of Oxone or Ce^{4+}.[15] While the exact role of the carboxylate during catalytic turnover has not been established, one

Received: March 20, 2013
Published: June 18, 2013

   dx.doi.org/10.1021/ic400691e | *Inorg. Chem.* 2013, 52, 7615−7622

possibility is that coordination of this anionic ligand may stabilize high-valent species to produce the reactive intermediate.

Deprotonated carboxamido groups are particularly strong donors and have also been shown to support isolable high-valent manganese compounds. The tetra-amido macrocyclic ligands (TAML) of Collins et al., with four carboxamido ligands in a square-planar arrangement, have been used to generate square pyramidal $Mn^{V}{\equiv}O$ species that are stable in air and water.[16,17] Similarly, Borovik and co-workers showed that three carboxamido ligands in a trigonal arrangement promote the formation of a high-spin Mn^{V}−oxo complex.[18] In both systems, the Mn^{V}−oxo species possess a strong, short Mn−O bond that is unreactive toward nucleophilic attack. For water oxidation, a reactive electrophilic Mn−oxo species is required, and thus the electron donor power of the ligand needs to be balanced to favor the formation of high-valent species that are also reactive. This application of the Sabatier principle has been applied in heterogeneous catalysis of water oxidation,[19,20] but to our knowledge no extensive systematic studies of electron donor capability have been done to parameterize the ligand effect in homogeneous water-oxidation catalysis. Additionally, the geometric arrangement of the ligand donor atoms may be of consequence for catalytic activity. In the Borovik[18] and Collins[16,17] systems, the carboxamido donor atoms are oriented *cis* to the site of the terminal oxo. The inclusion of a high *trans*-effect ligand like a carboxamido in the position *trans* to the terminal oxo site may favor a reactive species by lengthening and weakening the Mn−oxo bond.

In this study, we have sought to replace the μ-oxo bridging groups of the previous studies with a carboxamido donor group to generate a mononuclear manganese water-oxidation catalyst. Mononuclear iron, cobalt, ruthenium, and iridium water-oxidation catalysts[21−29] have been reported in the literature, but only one example of a mononuclear manganese water-oxidation catalyst is known.[30] In an attempt to overcome the inherent lability of Mn^{II}, complexes of the chelating pentadentate ligand $PaPy_3^-$ ($PaPy_3H$ = *N*,*N*-bis(2-pyridylmethyl)-amine-*N*-ethyl-2-pyridine-2-carboxamide) were studied. This ligand, developed by Mascharak and co-workers, integrates a single deprotonatable carboxamide poised to bind *trans* to the labile sixth coordination site.[31] The reactivity of the manganese complex of this ligand is compared to those of analogous complexes of the neutral pentadentate ligands N4Py (N4Py = *N*,*N*-bis(2-pyridylmethyl)-*N*-bis(2-pyridyl)methylamine) and PY5 (PY5 = 2,6-bis(bis(2-pyridyl)methoxymethane)-pyridine) (Figure 1).

Manganese complexes of $PaPy_3^-$,[32,33] N4Py,[34] and PY5[35] have been previously developed for other purposes. Here, the oxygen evolution activity of $[Mn(PaPy_3)(NO_3)](ClO_4)$ (**1**), $[Mn(PaPy_3)(\mu\text{-}O)(PaPy_3)Mn](ClO_4)_2$ (**2**), [Mn(N4Py)OTf](OTf) (**3**), and $[Mn(PY5)(OH_2)](ClO_4)_2$ (**4**) in the presence of Oxone and hydrogen peroxide is reported and compared. The reactivity of these compounds was further characterized by cyclic voltammetry (CV) and spectroscopy. In general, the inclusion of an X-type, N-donor ligand promotes the formation of a high-valent Mn species competent for O−O bond formation.

MATERIALS AND METHODS

General. Oxone ($2KHSO_5{\cdot}KHSO_4{\cdot}K_2SO_4$) was purchased from Sigma-Aldrich and standardized by iodometric titration. All other reagents were purchased from commercial suppliers and used without further purification unless indicated. Elemental analyses were performed by Atlantic Microlab, Inc. (Norcross, GA). All aqueous solutions were prepared using ultra high-purity water (18.2 MΩ cm).

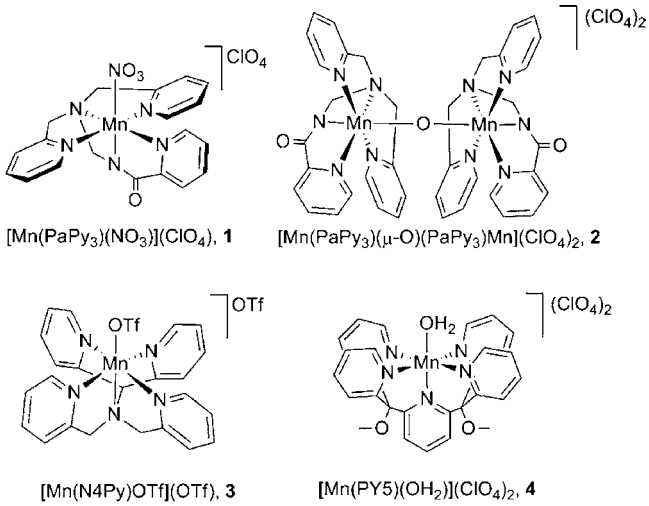

Figure 1. Manganese complexes investigated in this study.

Synthesis of Compounds. Ligands PY5[35] and $PaPy_3H$[31] and complexes $[Mn(PY5)(OH_2)](ClO_4)_2$[35] (**4**), $[Mn(PaPy_3)(OH_2)](ClO_4)$,[32] and $[Mn(PaPy_3)(\mu\text{-}O)(PaPy_3)Mn](ClO_4)_2$[33] (**2**) were prepared by methods published previously. [Mn(N4Py)OTf](OTf)[34] (**3**) was prepared as previously reported from commercially available $Mn(OTf)_2$ (Sigma-Aldrich). The synthesis of **3** was performed under nitrogen atmosphere with dry solvents because the final product was observed to be very hygroscopic.

Caution! *Perchlorate salts of metal complexes with organic ligands are potentially explosive and should be handled with care in small quantities.*

The N4Py ligand was prepared by a slight modification of a previously reported procedure.[36] A solution of 1.870 g (11.4 mmol) of 2-picolyl chloride HCl was stirred in 2.25 mL of 5 M aqueous NaOH at 0 °C for 10 min. A solution of 1.055 g (5.7 mmol) of di-2-pyridylmethanamine in 2.25 mL of 5 M aqueous NaOH was added. The reaction mixture was stirred at room temperature for 48 h. After this time, 1 equiv of concentrated HNO_3 (0.36 mL) was added. The reaction mixture was extracted with dichloromethane. The organic extracts were washed with $NaHCO_3$ solution and with brine, dried with $NaSO_4$, filtered, and evaporated. The resulting oil was purified by column chromatography on alumina with 0−25% methanol in dichloromethane as eluent. Characterization by NMR spectroscopy was consistent with literature data (yield 0.989 g, 47%).

$[Mn(PaPy_3)(NO_3)](ClO_4)$ (**1**) was prepared by adaptation of a literature procedure.[32] $[Mn(PaPy_3)(OH_2)](ClO_4)$ (105.6 mg, 0.21 mmol) was added to 30 mL of acetonitrile. After 30 min of stirring in air, the light brown suspension darkened to a dark brown solution, presumably $[Mn(PaPy_3)(\mu\text{-}O)(PaPy_3)Mn](ClO_4)_2$. After 4 h of stirring, HNO_3 (12 μL, 0.21 mmol) in 5 mL of acetonitrile was added, producing an emerald green solution within seconds. After an additional 1 h of stirring, the solution was concentrated to 5 mL in vacuo. Green plates of $[Mn(PaPy_3)(NO_3)](ClO_4)$ were grown by vapor diffusion of diethyl ether and isolated from a brown oil byproduct by filtration and washing with diethyl ether (yield 26.8 mg, 23%). Anal. Calcd for $C_{20}H_{20}ClMnN_6O_8{\cdot}0.5H_2O$: C 42.01; H 3.70; N 14.70. Found: C 42.05; H 3.76; N 14.78. Absorption spectrum (MeCN) λ_{max} (nm), ε (M^{-1} cm^{-1}): 647, 200; 430 (sh), 700.

Crystal Structure. Green plates of **1** suitable for single-crystal X-ray diffraction were grown overnight by diffusion of diethyl ether into an acetonitrile solution of **1** at 4 °C. Compound **1** crystallizes in the monoclinic space group $P2_1/c$ with one molecule in the asymmetric unit. Both the nitrate ligand and perchlorate anion were disordered over two positions. The occupancy of the two disordered groups refined to 0.764(6) and 0.746(10).

dx.doi.org/10.1021/ic400691e | *Inorg. Chem.* 2013, 52, 7615−7622

Low-temperature diffraction data (ω-scans) were collected on a Rigaku MicroMax-007HF diffractometer coupled to a Saturn994+ CCD detector with Cu Kα radiation (λ = 1.54178 Å) for the structure of **1**. The structure was solved by direct methods using SHELXS[37] and refined against F^2 on all data by full-matrix least-squares with SHELXL-97[38] using established refinement techniques.[39] All non-hydrogen atoms were refined anisotropically. All hydrogen atoms were included in the model at geometrically calculated positions and refined using a riding model. The isotropic displacement parameters of all hydrogen atoms were fixed to 1.2 times the U value of the atoms to which they are linked (1.5 times for methyl groups). The structure shows significant disorder that could not be completely modeled, and a correction for diffuse solvent was applied. All disorders were refined with the help of similarity restraints on the 1,2- and 1,3-distances and displacement parameters as well as rigid bond restraints for anisotropic displacement parameters. Additional experimental details and structural parameters are available in the Supporting Information.

O_2 Evolution Kinetics. Initial rates of O_2 evolution were measured using a YSI Standard Oxygen Probe (Clark electrode) fitted with a fresh Teflon FEP membrane and standardized by measuring the electrode response both of air-saturated water and of oxygen-depleted water prepared by addition of sodium bisulfite. In a typical experiment, 5 mL of an air-saturated aqueous solution of Oxone or hydrogen peroxide (10−250 mM) was stirred in a custom water-jacketed vessel maintained at 25 °C by a recirculating water bath. The electrode, secured in a Teflon tube, was inserted into the vessel such that no headspace existed between the solution and electrode. After 2−5 min of equilibration, indicated by a steady voltage reading, an aliquot (10−80 μL) of catalyst solution (2−4 mM) was injected. Initial rates were determined by a linear least-squares fit of the first minute of oxygen evolution. Michaelis−Menten analyses were completed using non-linear curve-fitting techniques implemented in Origin 9.0.

UV−Visible Spectrophotometry. UV−visible spectra were measured using a Cary 50 spectrophotometer. Spectra were baseline corrected with the pure solvent spectrum. Spectrophotometric titrations were performed using 0.4 M Britton−Robinson buffer[40] titrated with 2 M NaOH to minimize volume changes. The pH of the solution was recorded after each addition by a pH-sensitive electrode. Volume changes were recorded, and spectra were corrected to account for the change in concentration owing to dilution. The pK_a values were determined by the derivative method[41] of Irving et al. and compared to the result given by the absorbance ratio method[42] of Waring.

EPR Spectroscopy. Samples of **1** for electron paramagnetic resonance (EPR) spectroscopy were prepared by dissolving [Mn(PaPy$_3$)(NO$_3$)](ClO$_4$) in 0.1 M aqueous KNO$_3$ (1 mM) and loading 200 μL into a 4 mm outside diameter quartz tube. Samples of **1** in the presence of oxidant (Oxone or H_2O_2) were prepared by placing 100 μL of a 1 mM solution of [Mn(PaPy$_3$)(NO$_3$)](ClO$_4$) dissolved in 0.1 M aqueous KNO$_3$ at the bottom of a 4 mm o.d. EPR tube and freezing in liquid N_2. A 100 μL aliquot of oxidant solution (10 mM, 5 equiv) was layered over the frozen Mn solution. The frozen portion was allowed to thaw at room temperature to promote mixing, and then the sample was refrozen in liquid N_2 before insertion into the spectrometer. A standard curve of EPR intensities was determined by measuring the peak-to-peak amplitude of the EPR signal for a series of solutions of MnSO$_4$ of known concentration in 0.1 M aqueous KNO$_3$. EPR spectra were measured at 7 K in perpendicular mode on a Bruker ELEXYS E500 spectrometer equipped with an SHQ cavity and Oxford ESR 900 liquid helium cryostat with the following settings: microwave frequency = 9.391 GHz, microwave power = 0.5 mW, modulation frequency = 100 kHz, modulation amplitude = 10 G.

Electrochemistry. Electrochemical experiments were conducted with a Princeton Applied Research VersaSTAT 4 potentiostat/galvanostat using a standard three-electrode setup consisting of a basal plane graphite working electrode, a saturated Ag/AgCl reference electrode (BASi), and a platinum wire counter electrode (Strem). A basal plane graphite working electrode was polished with 1 μm alumina, rinsed with water, and allowed to dry before use. The surface of the electrode was resurfaced with tape to restore the gray, basal surface. Experiments were carried out in unbuffered 0.1 M aqueous KNO$_3$ (Johnson Matthey, electronics grade). In pH-dependent experiments, the pH was adjusted using HNO$_3$ or KOH. Measured potentials are referenced to normal hydrogen electrode (NHE) using the relation 0 V versus NHE = +0.197 V vs Ag/AgCl.

RESULTS

Preparation and Solution Properties of 1−4. To study the effect of adding an anionic ligand in the coordination sphere of Mn on oxygen evolution, the Mn complexes of neutral pentadentate ligands PY5 and N4Py were compared with the anionic pentadentate ligand PaPy$_3^-$. These complexes are known to be stable in air, but their behavior in aqueous solution was not previously reported.

[Mn^{III}(PaPy$_3$)(NO$_3$)](ClO$_4$) (**1**) was prepared by a slight modification of a previously reported synthesis.[32] In acetonitrile solution, [Mn^{II}(PaPy$_3$)(OH$_2$)](ClO$_4$) is oxidized in air to form [Mn(PaPy$_3$)(μ-O)(PaPy$_3$)Mn](ClO$_4$)$_2$ (**2**). The single μ-oxo bridge of this compound is susceptible to protonation by a variety of proton donors.[33] When HNO$_3$ is added to a dark brown solution of **2** in acetonitrile, the oxo bridge is protonated and the anionic NO$_3^-$ conjugate base replaces the bound water, producing an emerald green solution from which green crystals of the mononuclear complex **1** were obtained. Nitrate was chosen for this application because it is resistant to oxidation and weakly coordinating, creating a labile site for binding water or an oxidant. The crystal structure of **1** (see Supporting Information) is comparable to other structures of manganese bound to the PaPy$_3^-$ ligand, showing that the carboxamido nitrogen is coordinated *trans* to the labile inner sphere nitrate.[33]

When **1** or **2** is dissolved in water, an orange solution is produced, consistent with conversion of **1** or **2** to a new species in aqueous solution (Figure 2). The spectra are consistent with

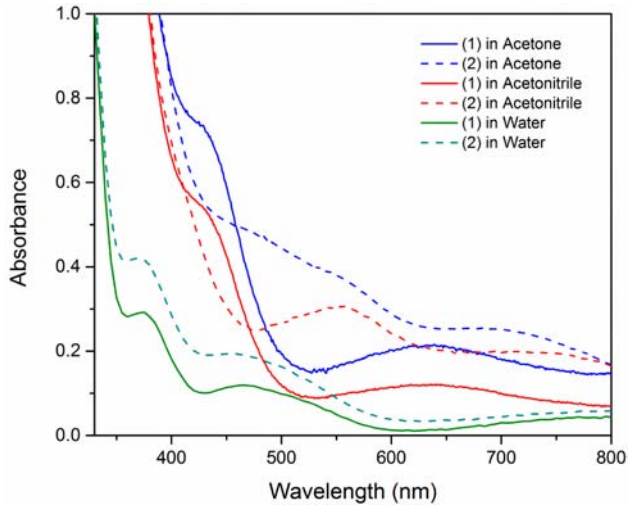

Figure 2. Absorbance spectra of **1** (solid lines) and **2** (dashed lines) in acetone (blue), acetonitrile (red), and water (green). Compounds **1** and **2** exhibit different absorbance features in nonaqueous solvents that converge to the same spectrum in aqueous solution.

Mn^{III} in either monomeric or oxo-bridged dimeric form.[43,44] The color of the solutions persists for weeks at room temperature, indicating stability of the complexes. The same absorbance spectrum is observed when an acetonitrile solution of **1** or **2** is titrated with water (see Supporting Information, Figures S1 and S2). While the spectrum of **2** changes to that of the aqueous species in 2% water in acetonitrile, **1** requires 12%

dx.doi.org/10.1021/ic400691e | Inorg. Chem. 2013, 52, 7615−7622

water in acetonitrile for complete conversion to the aqueous species, suggesting that it is harder to displace the nitrate ligand than to break the μ-oxo bridge. The similarity of the absorbance spectra would suggest that **1** and **2** form the same aqueous species. The weakly bound nitrate ligand in **1** may be replaced by a water molecule in aqueous solution, while the μ-oxo ligand of **2** is subject to protonation at intermediate pH.

Titration of **1** in aqueous Britton–Robinson buffer reveals that the complex is stable between pH 2 and 10.5 (Figure 3).

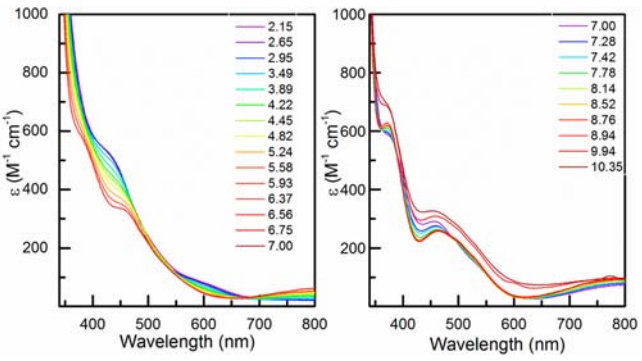

Figure 3. Spectrophotometric titration data of **1** in 0.04 M Britton–Robinson buffer with 2 M NaOH. The absorbance spectrum and pH were recorded after each addition. (Left) Titration of $[Mn(PaPy_3)(OH_2)]^{2+}$ to form $[Mn(PaPy_3)(OH)]^{+}$. (Right) Titration of $[Mn(PaPy_3)(OH)]^{+}$ to form $[(PaPy_3)Mn(\mu\text{-}O)Mn(PaPy_3)]^{2+}$. Spectra are normalized by concentration, accounting for the added volume during titration.

Below pH 2, the color of the solution slowly bleaches over several minutes, suggesting that the pentadentate ligand may be protonated and decoordinate from the metal. Above pH 10.5, solid MnO_2 is observed to precipitate from solution. Two pK_a transitions are observed in this range, and the speciation is shown in Scheme 1 (see also Suppporting Information, Figure

Scheme 1. Speciation of 1 in Aqueous Solution

$$[Mn(PaPy_3)(OH_2)]^{2+} \underset{}{\overset{pK_a\approx 5.0}{\rightleftharpoons}} [Mn(PaPy_3)(OH)]^{+}$$

$$[Mn(PaPy_3)(OH)]^{+} \overset{pK_a\approx 9.9}{\rightleftharpoons} [(PaPy_3)Mn(\mu\text{-}O)Mn(PaPy_3)]^{2+}$$

S3). As **1** is titrated from pH 2 to 7, the spectra exhibit an isosbestic point with a pK_a near 5.0 (Figure 3). This pK_a is assigned to the first deprotonation of the Mn-bound water molecule to form a coordinated hydroxide species, $[Mn^{III}(PaPy_3)(OH)]^{+}$. The second p$K_a$ is approximately 9.9, assigned to the second deprotonation of the Mn-bound water concomitant with formation of an oxide ligand to produce dimeric μ-oxo species. Titration through this pK_a also exhibits a few isosbestic points, shown in Figure 3. We have been unable to characterize these species formed in aqueous solution further using mass spectrometry or crystallography. While all observations indicate that **1** and **2** form the same species in aqueous solution, experiments will continue to be conducted based on the precursor material.

$[Mn^{II}(N4Py)OTf](OTf)$ (**3**) and $[Mn^{II}(PY5)(OH_2)](ClO_4)_2$ (**4**) are both stable in aqueous solution. **3** is very hygroscopic as a solid and becomes a brown oil when exposed to moist air. It is stable, however, when stored in a desiccator.

Oxygen Evolution. For the four manganese complexes in this study, the initial rate of oxygen evolution was measured using a Clark electrode. When an aqueous solution of **1** or **2** is injected into a solution containing Oxone, oxygen evolution commences immediately. Kinetic studies with **1** demonstrate that the reaction is first-order in manganese (Supporting Information, Figure S4). At concentrations of Oxone above 100 mM, the initial rate saturates (Figure 4). By comparison, **3**

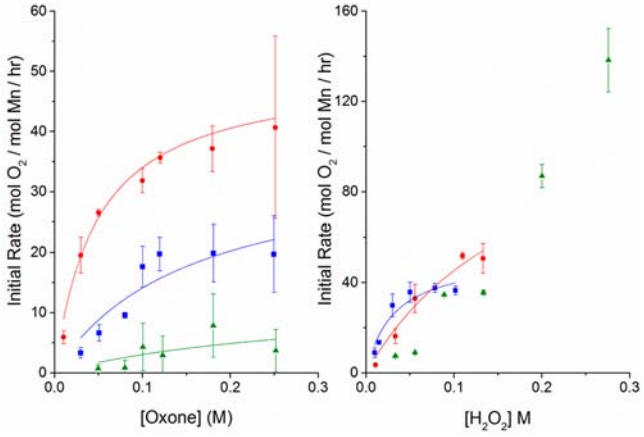

Figure 4. Effect of varying $[HSO_5^-]$ (left) and $[H_2O_2]$ (right) on the initial rate of oxygen evolution from **1** (blue), **2** (red), and **3** (green). Rate values are normalized by the moles of Mn in each sample (4 mM). Reported errors are one standard deviation from the average of all measurements carried out at each concentration.

catalyzes oxygen evolution more slowly; at Oxone concentrations less than 50 mM, the rate of oxygen evolution is difficult to distinguish from the background. When **4** was injected into a solution containing Oxone, no oxygen evolution was observed above background within 10 min.

Oxygen evolution is also observed if a solution of **1** or **2** is injected into a solution containing hydrogen peroxide. Manganese complexes commonly catalyze the dismutation of hydrogen peroxide, the same reaction catalyzed by the enzyme manganese catalase.[45] Like the reaction with Oxone, the rate of this reaction catalyzed by **1** or **2** saturates at hydrogen peroxide concentrations above 100 mM. Complex **3** is observed to evolve oxygen in the presence of H_2O_2, but the initial rate does not saturate even at 275 mM H_2O_2 (>7700 equiv). No oxygen evolution is observed above baseline when **4** is injected into a solution containing H_2O_2.

The initial rates of oxygen evolution for each complex were normalized by moles of Mn in solution and fit as a function of oxidant concentration (Figure 4). The data were modeled by the Michaelis–Menten equation, and a comparison of the extracted V_{max} and K_m parameters is shown in Table 1. As shown in Table 1, the reported rates of oxygen evolution in the presence of Oxone catalyzed by **1** and **2** are the same within error, while the rate for **3** is significantly lower. The discrepancy between the measured rates for **1** and **2** below saturation is attributed to experimental variations in the measurement of oxygen evolution using a Clark electrode.

The initial rates were calculated from a linear fit of the first 60 s of data, but oxygen evolution continues for only a few minutes. The total number of turnovers is low, only 3 or 4, depending on the Oxone concentration, before the oxygen evolution ceases. The low turnover number suggests that decomposition of the complex is competitive with catalysis.

dx.doi.org/10.1021/ic400691e | Inorg. Chem. 2013, 52, 7615–7622

Table 1. Kinetic Data Calculated from Figure 4

catalyst precursor	oxidant	V_{max}[a] (mol of O_2 (mol of Mn)$^{-1}$ h^{-1})	K_m[a] (mM)
$[Mn^{III}(PaPy_3)(NO_3)](ClO_4)$, **1**	Oxone	35.7 ± 12.4	153 ± 104
$[Mn^{III}(PaPy_3)(\mu\text{-}O)(PaPy_3)Mn^{III}](ClO_4)_2$, **2**	Oxone	50.2 ± 4.1	48 ± 9
$[Mn^{II}(N4Py)(OTf)](OTf)$, **3**	Oxone	12.3 ± 1.7	306 ± 796
$[Mn^{II}(PY5)(OH_2)](ClO_4)_2$, **4**	Oxone	none	none
$[Mn^{III}(PaPy_3)(NO_3)](ClO_4)$, **1**	H_2O_2	52.1 ± 8.1	31 ± 12
$[Mn^{III}(PaPy_3)(\mu\text{-}O)(PaPy_3)Mn^{III}](ClO_4)_2$, **2**	H_2O_2	132 ± 58	191 ± 128
$[Mn^{II}(N4Py)(OTf)](OTf)$, **3**	H_2O_2	–[b]	–[b]
$[Mn^{II}(PY5)(OH_2)](ClO_4)_2$, **4**	H_2O_2	none	none

[a]Calculated from Michaelis–Menten fit of data. [b]No comparison is available because the initial rate does not saturate at high H_2O_2 concentration.

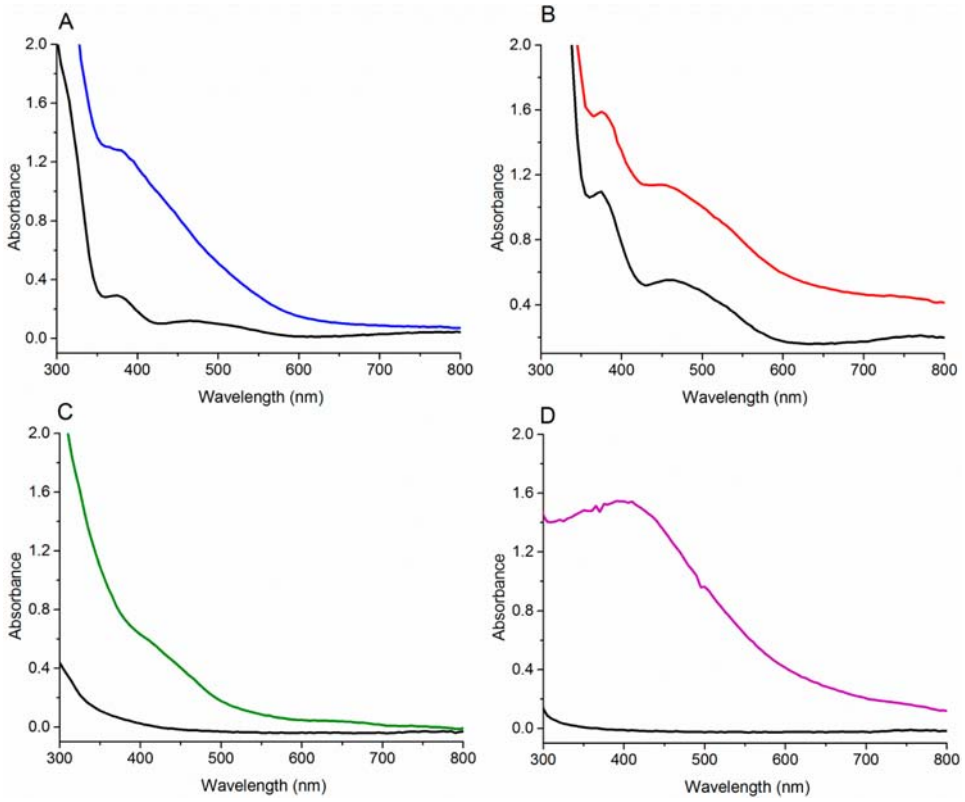

Figure 5. Absorbance spectra before (black) and after (color) addition of 1 equiv of Oxone showing the formation of stable high-valent Mn species for **1** (A, blue), **2** (B, red), **3** (C, green), and **4** (D, violet).

The mechanisms of degradation may include oxidation of the ligand to produce a different complex or an inactive manganese oxide material.

UV–Visible Spectroscopy. To investigate which species are involved in the dioxygen evolution, the reaction was studied using UV–visible spectrophotometry and EPR spectroscopy. The absorbance spectra of **1**–**4** in water were collected before and after the addition of 1 equiv of Oxone (Figure 5). In general, the peaks at 375 and 465 nm in the spectra of **1** and **2** were replaced within a few seconds of Oxone addition by new features with a higher molar absorptivity. In the spectrum of **1**, the new spectrum consists of a broad shoulder at 380 nm, while the spectrum of **2** with Oxone exhibits two features at 380 and 450 nm. The increase in molar absorptivity is consistent with oxidation to Mn^{III} or Mn^{IV}, characterized by a ligand-to-Mn charge transfer band in the visible spectrum.[46] A solution of **3** also increases in absorbance upon addition of Oxone over 5 min. Similarly, addition of Oxone to a solution of **4** produced a new absorbance at 410 nm, indicating generation of a high-valent Mn species. However, the oxidized species from **4** forms slowly over 30 min, after which the solution becomes turbid, resulting from MnO_2 particle formation.

EPR Spectroscopy. The absorbance spectrum was compared with the results of EPR spectroscopy in perpendicular mode to determine the possible oxidation states. The spectrum of **1** collected in frozen 0.1 M aqueous KNO_3 at 7 K indicates the formation of a small amount of Mn^{II} impurity indicated by the broad, six-line signal at g = 2 (Supporting Information, Figure S5). This signal is typical of high-spin Mn(II) (S = 5/2) with coupling to ^{55}Mn (I = 5/2). The broadness of the peaks is consistent with unresolved zero-field splitting observed in lower than octahedral symmetry. Quantification of Mn^{II} by comparison to a standard curve of known concentrations indicates that approximately 16% of total Mn is represented by this signal. The remainder of the Mn is in a configuration that is EPR-silent in perpendicular mode, consistent with the Mn^{III} species suggested by the UV–visible absorbance data.

dx.doi.org/10.1021/ic400691e | Inorg. Chem. 2013, 52, 7615–7622

When a solution containing 5 equiv of Oxone is added to **1** and the mixture is frozen within 10 s of mixing, the Mn^{II} signal increases in intensity. After 10 s, 28% of the total manganese is reduced to Mn^{II} by comparison to a standard curve, and this signal likely originates from the reduction or disproportionation of reactive high-valent intermediates. If the solution is allowed to stand at room temperature for 10 min, 34% of the Mn in the sample has been converted to Mn^{II}. The oxidation of low-valent Mn to the high-valent states appears to be slow, resulting in a steady-state concentration of Mn^{II} in the presence of Oxone. The remainder of the Mn in the sample is in EPR-silent configurations, such as the Mn^{III} starting species or a Mn^{IV}/Mn^{IV} dimer suggested by the absorbance spectra. Notably, no Mn^{III}/Mn^{IV} mixed-valence species characterized by a 16-line spectrum centered at $g = 2$ is observed, even 10 min after mixing. Likewise, no mononuclear Mn^{IV}, which would be expected to have a feature at $g = 4$, is observed.

Electrochemistry. In order to compare the potentials at which the observed high-valent intermediates form, the aqueous electrochemical properties of complexes **1**, **3**, and **4** were investigated in 0.1 M KNO_3 electrolyte between +0.2 and +1.5 V versus NHE, and the cyclic voltammograms are shown in Figure 6.

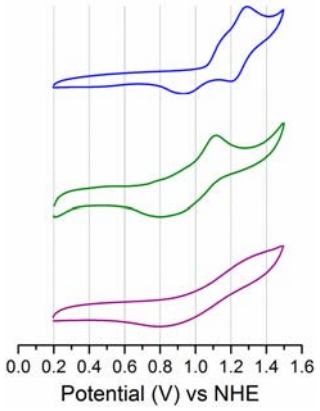

Figure 6. Cyclic voltammograms of **1** (top), **3** (middle), and **4** (bottom) from +0.2 to +1.5 V vs NHE in 0.1 M aqueous KNO_3. The scan rate is 50 mV/s. Vertical lines are drawn to facilitate comparison of potentials.

In the cyclic voltammogram of **1**, two quasireversible features were observed between +0.2 and +1.5 V (Figure 6, top). The first oxidation occurs at +1.18 V and is related to the return feature at +0.95 V. If this wave is isolated, it is quasireversible with a midpoint potential of +1.03 V and peak separation of 82 mV (Supporting Information, Figure S6). This feature is attributed to oxidation of Mn^{II} to Mn^{III}. The second couple at $E_{1/2}$ = +1.25 V is nearly reversible with a peak separation of 70 mV. The pH-dependent CV data, shown in Figure 7, indicate that the first couple is dependent on pH, while the second couple is independent of pH. However, the pH dependence of the first oxidation feature is not a simple shift in potential expected for a proton-coupled electron transfer process. Similarly, the intensity, but not the potential, of the return wave at +0.95 is pH-dependent. This complex behavior is indicative of a pH-dependent speciation. If the equilibria shown in Scheme 1 are fast compared to the electrochemical time scale, then the second oxidation may be the oxidation of the $Mn^{III}-O-Mn^{III}$ dimer to a $Mn^{III}-O-Mn^{IV}$ species with no net

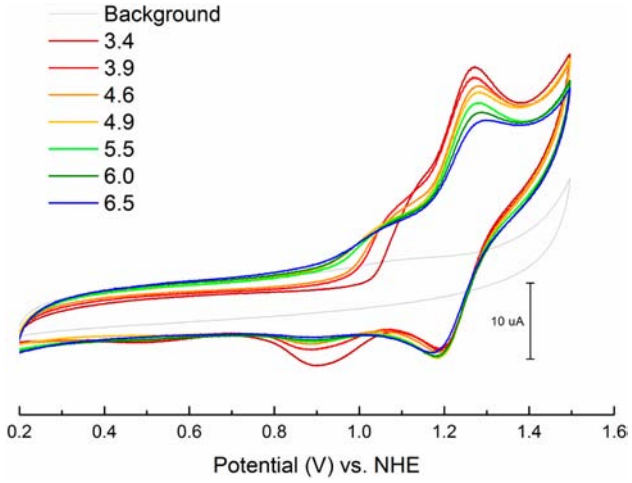

Figure 7. pH-dependent CV data of **1** in 0.1 M aqueous KNO_3 from pH 3.4 (red) to pH 6.5 (blue) in ~0.5 pH unit increments.

deprotonation. While the potential of the Mn^{III}/Mn^{IV} couple for the monomeric species may be above +1.5 V, the oxo bridge in the dimeric species stabilizes the high-valent state, making oxidation accessible. The dimeric species is expected to be present only at very low concentrations between pH 3.5 and 6.5, but oxidation shifts the equilibrium so that this redox couple is observed. The aqueous electrochemistry of a solution of **2** is identical to that of **1**, supporting this interpretation.

CV data of **3** under the same conditions exhibit an anodic peak at +1.11 V and a broad cathodic peak at +0.80 V (Figure 6, middle). Upon subsequent scans, the capacitance of the sample increases, indicating deposition of material on the electrode surface. A scan of the electrode in 0.1 M aqueous KNO_3 after cycling in a solution of **3** reveals new features consistent with decomposition of the Mn complex to manganese oxide under electrochemical oxidation (Supporting Information, Figure S7). No such buildup is observed for **1** above pH 7. This comparison suggests that the $PaPy_3^-$ ligand is more tightly bound than the N4Py ligand. The cylic voltammogram of **4** is similar to that of **3**, displaying one quasireversible feature, but the oxidation feature is at higher potential, +1.33 V (Figure 6, bottom). The reduction feature is similar, near +0.84 V. The CV data of **4** are attributed to the Mn^{II}/Mn^{III} couple, consistent with a previous report that a quasireversible peak at +1.260 V versus NHE for this compound in acetonitrile is lowered to +0.805 V in the presence of a base.[35]

■ DISCUSSION

The ligands PY5, N4Py, and $PaPy_3H$ consist of five N-donor atoms poised for coordination to a single transition metal center. PY5 and N4Py both contain only L-type nitrogen ligands from pyridyl groups or tertiary amines. By contrast, the N-donors in $PaPy_3H$ include three pyridine donors and a tertiary amine as well as a deprotonatable carboxamide. Mascharak and co-workers observe that the amide nitrogen atom binds *trans* to the sixth ligand site as an X-type carboxamido to Mn as long as a base is present to accept the proton from the amide,[32] in agreement with the structure of $[Mn(PaPy_3)(NO_3)](ClO_4)$ reported here.

Electronically, the PY5 and N4Py ligands are similar, while the $PaPy_3^-$ ligand is significantly more σ-donating. This trend is readily observable in the preparation of the compounds. The

dx.doi.org/10.1021/ic400691e | *Inorg. Chem.* 2013, 52, 7615−7622

complexes of the neutral ligands are stable as Mn^{II} while the Mn complex of $PaPy_3^-$ readily forms Mn^{III} in air, consistent with the increased electron density stabilizing a higher-valent species. $[Mn^{III}(PY5)(OH)](ClO_4)_2$ may be prepared by oxidation of **4** by iodosylbenzene.[35] This complex is stable in air but rapidly decomposes in water to precipitate manganese dioxide. The relative instability of the Mn^{III} complex of PY5 compared to that of $PaPy_3^-$ demonstrates how a carboxamido group may be used to stabilize high-valent manganese species in water. The cyclic voltammetry data in Figure 6 suggest that the Mn^{II} form of complex **1** is oxidized to higher-valent states at a potential comparable to complex **3** and at a potential lower than **4**. Furthermore, the subsequent oxidation of **1** to a Mn^{III}/Mn^{IV} species is observed at potentials within the electrochemical window, whereas only one oxidation is observed for **3** or **4**. While **4** is reported to oxidize weak C−H and O−H bonds in acetonitrile,[35] it appears that the PY5 ligand does not sufficiently stabilize Mn^{III} to allow access to oxidizing higher-valent species. Water oxidation is reported for the cobalt analog of **4**, but only in the pH range of 7.6−10.3 where water oxidation is more thermodynamically favorable.[27,28]

The electronic effect of the $PaPy_3^-$ ligand may promote water oxidation by orienting the carboxamido group *trans* to the site of water binding. The *trans* effect may discourage the formation of the bridging oxo group in **1** and **2**, allowing faster ligand exchange at the open site compared to that of **3** or **4**. The absorbance spectra in Figure 5 are consistent with this observation, showing that oxidation occurs quickly for **1** and **2** but is slower for **3** and **4**. In the previously reported Mn complexes of other carboxamido ligands, the anionic N-donors are oriented *cis* to the Mn−oxo, resulting in high-valent but unreactive compounds.[17,47] High *trans*-effect ligands such as the carboxamido nitrogen have been suggested in the literature to favor reactive end-on peroxo formation in the presence of H_2O_2 over comparatively stable and unreactive side-on peroxo binding.[34,48]

The effect of the anionic N-donor ligand is most apparent in the comparison of the rate of oxygen evolution. The oxygen evolution activity of **1** and **2** using Oxone as the primary oxidant is much greater than that of **3**. Though the exact structures of the active species have not been characterized, the expected mechanism involves binding of Oxone to generate a high-valent Mn species.[10] This postulated intermediate may further react with either water or a second equivalent of Oxone to form an O−O bond to produce O_2. The greater reactivity of **1** and **2** compared to that of **3** indicates that the reactive species required for O−O bond formation is accessible by reaction with Oxone when the high-valent species is sufficiently stabilized. For **3** and **4**, the oxidizing potential required to produce the O−O bond-forming intermediate is not accessible with Oxone (E° = +1.81 V vs NHE).[49] However, the UV−visible absorbance spectra in Figure 5 indicate that **3** and **4** both slowly form high-valent species in the presence of Oxone. One possibile explanation for this behavior is that achieving a stable high-valent state for these compounds requires formation of a μ-oxo bridge between the metal centers. In the case of **1** and **2**, the anionic ligand promotes rapid formation and exchange of the stabilizing μ-oxo bridge, but **3** and **4** react with the oxidant much more slowly.

Unlike **4**, complex **3** does produce oxygen in the presence of Oxone, albeit slowly. The cause of this modest reactivity may be due to the greater conformational flexibility of the N4Py ligand compared to that of the PY5 ligand. The possibility of decoordination of one or more pyridine ligands may allow the formation of a dinuclear species bridged by μ-oxo ligands. This behavior is supported by an observation in a previous study that one of the pyridyl arms of the N4Py ligand of complex **3** decoordinates to form a side-on $[Mn-O_2]^+$ species upon reaction with hydrogen peroxide in acetonitrile at low temperature.[34] Direct structural confirmation of partial ligand decoordination in solution is difficult to obtain, and time-dependent density functional theory calculations were used to aid in interpretation of the spectroscopic data. However, the greater flexibility may also result in complete loss of the ligand to form free Mn^{2+} that may be oxidized to MnO_2. Decomposition of this complex to a heterogeneous material under oxidative conditions is consistent with the formation of a deposit on the electrode surface after cyclic voltammetry as well as the absence of saturation kinetics in the disproportionation of H_2O_2.

Some decoordination behavior is also possible with **1** and **2**.[32] However, the faster rate of oxygen evolution compared to those of the complexes of neutral ligands indicates that some of the increased reactivity must be due to the electronic influence of the bound anionic ligand. Also, no evidence of MnO_2 formation has been observed below pH 10.5 for **1** or **2**, indicating that the ligand remains at least partially coordinated. The formation of bridging species under oxidative conditions is suggested by the cyclic voltammetry experiments, but EPR spectroscopy demonstrates that no mixed-valent dinuclear Mn^{III}/Mn^{IV} species is formed in the steady state in the presence of Oxone, even at longer times as previously observed for $[Mn_2(tpy)_2(\mu\text{-}O)(OH_2)]_2(NO_3)_3$.[10] However, with partial dissociation of the ligand, a dinuclear Mn^{IV} species may be stabilized by two μ-O groups. This species would be expected to be EPR-silent at low temperature because of antiferromagnetic coupling of the manganese. The absorbance spectra in the presence of Oxone are consistent with Mn^{IV}, but a mononuclear Mn^{IV} species is not detected by EPR. These observations point to the formation of a coordinatively saturated and thus catalytically inactive $Mn^{IV}-(\mu\text{-}O)_2-Mn^{IV}$ species in the steady state similar to that formed by the manganese−terpyridine system.[10] However, the exact structure of the catalytic species is unclear.

An important concern is the possibility of ligand oxidation leading to catalyst degradation. The low turnover numbers suggest that the active catalyst is subject to a rapid degradation process. Although no MnO_2 is observed, it is possible that a very small amount of a highly active heterogeneous material could be responsible for the observed activity of **1** or **2**. However, manganese oxides are poor catalysts for oxygen evolution in the presence of Oxone,[10] so it is unlikely that a heterogeneous material is the true catalyst in this case.

When the rates of oxygen evolution catalyzed by **1** or **2** are compared to those of other Mn complexes, it is clear that this complex is less efficient than previously reported catalysts. Under similar conditions, $[Mn_2(tpy)_2(\mu\text{-}O)_2](NO_3)_2$ has a V_{max} of 2420 mol of O_2 (mol of Mn)$^{-1}$ h^{-1}.[9] The lower turnover frequencies of the compounds in this study may result from the use of a pentadentate ligand that leaves only one open site. Coordinatively saturated intermediates such as the Mn−O−Mn species suggested by the absorbance and EPR data represent unproductive pathways in the catalytic cycle. This may explain why PSII and manganese catalase require more than one metal center and why mononuclear manganese water-oxidation catalysts are not common in the literature.

dx.doi.org/10.1021/ic400691e | *Inorg. Chem.* 2013, 52, 7615−7622

CONCLUSIONS

In this study, we have compared the activities of four manganese complexes as catalysts for oxygen evolution with Oxone and hydrogen peroxide. Inclusion of an anionic carboxamido ligand *trans* to the labile coordination site promotes the formation of a high-valent Mn species competent for oxygen formation. This study suggests that incorporation of X-type ligands that are not subject to protonation during the catalytic cycle is a useful strategy for designing manganese-based water-oxidation catalysts.

ASSOCIATED CONTENT

Supporting Information

Additional absorbance spectra, EPR spectra, kinetic data, and crystallographic information for **1** as well as cyclic voltammetry data for **3**. This material is available free of charge via the Internet at http://pubs.acs.org.

AUTHOR INFORMATION

Corresponding Author

*E-mail: gary.brudvig@yale.edu. Phone: 203-432-5202. Fax: 203-432-6144.

Notes

The authors declare no competing financial interest.

ACKNOWLEDGMENTS

This work was supported by the Chemical Sciences, Geosciences, and Biosciences Division, Office of Basic Energy Sciences, Office of Science, U.S. DOE (DE-FG02-07ER15909). Special thanks to Professor Robert H. Crabtree for helpful comments.

REFERENCES

(1) McEvoy, J. P.; Brudvig, G. W. *Chem. Rev.* **2006**, *106*, 4455.
(2) Sproviero, E. M.; Gascón, J. A.; McEvoy, J. P.; Brudvig, G. W.; Batista, V. S. *J. Am. Chem. Soc.* **2008**, *130*, 3428.
(3) Walter, M. G.; Warren, E. L.; McKone, J. R.; Boettcher, S. W.; Mi, Q.; Santori, E. A.; Lewis, N. S. *Chem. Rev.* **2010**, *110*, 6446.
(4) Young, K. J.; Martini, L. A.; Milot, R. L.; Snoeberger, R. C., III; Batista, V. S.; Schmuttenmaer, C. A.; Crabtree, R. H.; Brudvig, G. W. *Coord. Chem. Rev.* **2012**, *256*, 2503.
(5) Cady, C. W.; Crabtree, R. H.; Brudvig, G. W. *Coord. Chem. Rev.* **2008**, *252*, 444.
(6) Wiechen, M.; Berends, H.-M.; Kurz, P. *Dalton Trans.* **2012**, *41*, 21.
(7) Karlsson, E. A.; Lee, B.-L.; Åkermark, T.; Johnston, E. V.; Kärkäs, M. D.; Sun, J.; Hansson, Ö.; Bäckvall, J.-E.; Åkermark, B. *Angew. Chem., Int. Ed.* **2011**, *50*, 11715.
(8) Limburg, J.; Vrettos, J. S.; Liable-Sands, L. M.; Rheingold, A. L.; Crabtree, R. H.; Brudvig, G. W. *Science* **1999**, *283*, 1524.
(9) Limburg, J.; Vrettos, J. S.; Chen, H.; de Paula, J. C.; Crabtree, R. H.; Brudvig, G. W. *J. Am. Chem. Soc.* **2001**, *123*, 423.
(10) Chen, H. Y.; Tagore, R.; Olack, G.; Vrettos, J. S.; Weng, T. C.; Penner-Hahn, J.; Crabtree, R. H.; Brudvig, G. W. *Inorg. Chem.* **2007**, *46*, 34.
(11) Siegbahn, P. E. M. *Inorg. Chem.* **2008**, *47*, 1779.
(12) Lomoth, R.; Huang, P.; Zheng, J.; Sun, L.; Hammarström, L.; Åkermark, B.; Styring, S. *Eur. J. Inorg. Chem.* **2002**, *2002*, 2965.
(13) Poulsen, A. K.; Rompel, A.; McKenzie, C. J. *Angew. Chem., Int. Ed.* **2005**, *44*, 6916.
(14) Seidler-Egdal, R. K.; Nielsen, A.; Bond, A. D.; Bjerrum, M. J.; McKenzie, C. J. *Dalton Trans.* **2011**, *40*, 3849.
(15) Berggren, G.; Thapper, A.; Huang, P.; Kurz, P.; Eriksson, L.; Styring, S.; Anderlund, M. F. *Dalton Trans.* **2009**, 10044.
(16) Collins, T. J.; Gordon-Wylie, S. W. *J. Am. Chem. Soc.* **1989**, *111*, 4511.
(17) Collins, T. J.; Powell, R. D.; Slebodnick, C.; Uffelman, E. S. *J. Am. Chem. Soc.* **1990**, *112*, 899.
(18) Taguchi, T.; Gupta, R.; Lassalle-Kaiser, B.; Boyce, D. W.; Yachandra, V. K.; Tolman, W. B.; Yano, J.; Hendrich, M. P.; Borovik, A. S. *J. Am. Chem. Soc.* **2012**, *134*, 1996.
(19) Bockris, J. O. M.; Otagawa, T. *J. Electrochem. Soc.* **1984**, *131*, 290.
(20) Suntivich, J.; May, K. J.; Gasteiger, H. A.; Goodenough, J. B.; Shao-Horn, Y. *Science* **2011**, *334*, 1383.
(21) Concepcion, J. J.; Jurss, J. W.; Templeton, J. L.; Meyer, T. J. *J. Am. Chem. Soc.* **2008**, *130*, 16462.
(22) Tseng, H.-W.; Zong, R.; Muckerman, J. T.; Thummel, R. *Inorg. Chem.* **2008**, *47*, 11763.
(23) Hull, J. F.; Balcells, D.; Blakemore, J. D.; Incarvito, C. D.; Eisenstein, O.; Brudvig, G. W.; Crabtree, R. H. *J. Am. Chem. Soc.* **2009**, *131*, 8730.
(24) Concepcion, J. J.; Jurss, J. W.; Norris, M. R.; Chen, Z.; Templeton, J. L.; Meyer, T. J. *Inorg. Chem.* **2010**, *49*, 1277.
(25) Blakemore, J. D.; Schley, N. D.; Balcells, D.; Hull, J. F.; Olack, G. W.; Incarvito, C. D.; Eisenstein, O.; Brudvig, G. W.; Crabtree, R. H. *J. Am. Chem. Soc.* **2010**, *132*, 16017.
(26) Fillol, J. L.; Codola, Z.; Garcia-Bosch, I.; Gomez, L.; Pla, J. J.; Costas, M. *Nat. Chem.* **2011**, *3*, 807.
(27) Wasylenko, D. J.; Ganesamoorthy, C.; Borau-Garcia, J.; Berlinguette, C. P. *Chem. Commun.* **2011**, *47*, 4249.
(28) Wasylenko, D. J.; Palmer, R. D.; Schott, E.; Berlinguette, C. P. *Chem. Commun.* **2012**, *48*, 2107.
(29) Hetterscheid, D. G.; Reek, J. N. *Angew. Chem., Int. Ed.* **2012**, *51*, 9740.
(30) Gao, Y.; Liu, J.; Wang, M.; Na, Y.; Åkermark, B.; Sun, L. *Tetrahedron* **2007**, *63*, 1987.
(31) Rowland, J. M.; Olmstead, M.; Mascharak, P. K. *Inorg. Chem.* **2001**, *40*, 2810.
(32) Ghosh, K.; Eroy-Reveles, A. A.; Avila, B.; Holman, T. R.; Olmstead, M. M.; Mascharak, P. K. *Inorg. Chem.* **2004**, *43*, 2988.
(33) Ghosh, K.; Eroy-Reveles, A. A.; Olmstead, M. M.; Mascharak, P. K. *Inorg. Chem.* **2005**, *44*, 8469.
(34) Geiger, R. A.; Leto, D. F.; Chattopadhyay, S.; Dorlet, P.; Anxolabehére-Mallart, E.; Jackson, T. A. *Inorg. Chem.* **2011**, *50*, 10190.
(35) Goldsmith, C. R.; Cole, A. P.; Stack, T. D. P. *J. Am. Chem. Soc.* **2005**, *127*, 9904.
(36) Lubben, M.; Meetsma, A.; Wilkinson, E. C.; Feringa, B.; Que, L. *Angew. Chem., Int. Ed. Engl.* **1995**, *34*, 1512.
(37) Sheldrick, G. *Acta Crystallogr., Sect. A* **1990**, *46*, 467.
(38) Sheldrick, G. *Acta Crystallogr., Sect. A* **2008**, *64*, 112.
(39) Müller, P. *Crystallogr. Rev.* **2009**, *15*, 57.
(40) Britton, H. T. S.; Robinson, R. A. *J. Chem. Soc.* **1931**, 1456.
(41) Irving, H.; Rossotti, H. S.; Harris, G. *Analyst (Cambridge, U.K.)* **1955**, *80*, 83.
(42) Waring, A. J. *Anal. Chim. Acta* **1983**, *153*, 213.
(43) Brunold, T. C.; Gamelin, D. R.; Stemmler, T. L.; Mandal, S. K.; Armstrong, W. H.; Penner-Hahn, J. E.; Solomon, E. I. *J. Am. Chem. Soc.* **1998**, *120*, 8724.
(44) Sheats, J. E.; Czernuszewicz, R. S.; Dismukes, G. C.; Rheingold, A. L.; Petrouleas, V.; Stubbe, J.; Armstrong, W. H.; Beer, R. H.; Lippard, S. J. *J. Am. Chem. Soc.* **1987**, *109*, 1435.
(45) Pecoraro, V. L.; Baldwin, M. J.; Gelasco, A. *Chem. Rev.* **1994**, *94*, 807.
(46) Gamelin, D. R.; Kirk, M. L.; Stemmler, T. L.; Pal, S.; Armstrong, W. H.; Penner-Hahn, J. E.; Solomon, E. I. *J. Am. Chem. Soc.* **1994**, *116*, 2392.
(47) Gupta, R.; Borovik, A. S. *J. Am. Chem. Soc.* **2003**, *125*, 13234.
(48) Annaraj, J.; Cho, J.; Lee, Y.-M.; Kim, S. Y.; Latifi, R.; de Visser, S. P.; Nam, W. *Angew. Chem., Int. Ed.* **2009**, *48*, 4150.
(49) Spiro, M. *Electrochim. Acta* **1979**, *24*, 313.